POLITECNICO DI TORINO
Repository ISTITUZIONALE

Quaternised Diels–Alder polyphenylene anion exchange membranes for efficient CO2 electrolysis

Original
Quaternised Diels–Alder polyphenylene anion exchange membranes for efficient CO2 electrolysis / Parata, C., Akouros, A., Theodoropoulos, N., Sacco, A., Zeng, J., Dante, S., Bexis, P., Paloumpis, G., De Castro, E.S., Zogali, V.. - In: JOURNAL OF MEMBRANE SCIENCE. - ISSN 0376-7388. - 762:(2027), pp. 1-12. [10.1016/j.memsci.2026.126301]

Availability:
This version is available at: 11583/3016931 since: 2026-10-24T16:30:21Z

Publisher:
Elsevier

Published
DOI:10.1016/j.memsci.2026.126301

Terms of use:

This article is made available under terms and conditions as specified in the corresponding bibliographic description in the repository

Publisher copyright

(Article begins on next page)

21 November 2026

Journal of Membrane Science 762 (2027) 126301

Contents lists available at ScienceDirect

Journal of Membrane Science

journal homepage: www.elsevier.com/locate/memsci

Quaternised Diels–Alder polyphenylene anion exchange membranes for efficient CO_2 electrolysis

Carmelo Parata [a,b,*], Antonios Akouros [b], Nikolas Theodoropoulos [b], Adriano Sacco [c], Juqin Zeng [a,c], Silvia Dante [d], Panagiotis Bexis [e], George Paloumpis [b], Emory S. De Castro [b], Vasiliki Zogali [b,**]

[a] Department of Applied Science and Technology (DISAT), Politecnico di Torino, Corso Duca Degli Abruzzi 24, Turin, 10129, Italy
[b] Advent Technologies, Stadiou, Platani, Patra, 26504, Greece
[c] Istituto Italiano di Tecnologia - IIT, Centre for Sustainable Future Technologies (CSFT), Via Livorno 60, Turin, 10144, Italy
[d] Istituto Italiano di Tecnologia - IIT, Via Morego, 30, Genova, GE, 16163, Italy
[e] Los Alamos National Laboratory, New Mexico, Los Alamos, NM, 87545, USA

ARTICLE INFO

Keywords:
Diels-alder polyphenylene
Anion exchange membrane
CO_2 electrolysis
Microphase separation
Chain entanglement

ABSTRACT

The membrane-electrode assembly (MEA) is a highly promising configuration for CO_2 reduction reaction with anion-exchange membranes (AEMs) playing a crucial role in limiting ion crossover, increasing operational time, and maintaining low cell voltage. In this study, we investigated Diels-Alder polyphenylenes (DAPP) functionalised with five distinct combinations of quaternary ammoniums and spacers to evaluate their impact on membrane properties and performance. Comprehensive characterisation, including thermal and alkaline stability, small-angle X-ray scattering, ion exchange capacity, water uptake, and swelling ratio, was combined with MEA electrolysis testing up to 65 h, alongside analysis of gaseous and liquid reduction products. Linear side-chain membranes (6C-TMA-DAPP and 6C-PIP-DAPP) exhibited superior alkaline stability and robust MEA performance, with 6C-PIP-DAPP achieving the best operational metrics and performing comparably to state-of-the-art AEMs. In contrast, branched side-chain membranes (5C-A-PIP-DAPP, 7C-A-PIP-DAPP and 9C-A-PIP-DAPP) displayed reduced alkaline stability and unusual voltage behaviours, likely related to restricted side-chain rotational freedom and altered polymer microstructure. These findings elucidate the importance of side-chain architecture on AEM performance, showing that linear side chains are well-suited for CO_2RR and providing new insights into AEM behaviour.

1. Introduction

In recent times, significant interest has been given to CO_2 electrolysis as a sustainable approach to mitigate the excess of atmospheric CO_2 while producing value-added chemicals and fuels. By utilising electricity derived from renewable sources such as solar energy, CO_2 electrolysis converts carbon dioxide into high-energy molecules, enabling renewable energy storage in chemical form [1]. Specifically, interest is focused on membrane electrode assembly (MEA) electrolysers, which are a setup able to limit ohmic losses to a minimum and enable operation at higher current densities suitable for commercial applications [2,3]. MEAs utilise ion-exchange membranes that separate the anode and cathode compartments and minimise product crossover, preventing back-reactions like reoxidation. Membranes are core components of the MEA and an impactful factor in many of the characteristics of the electrolyser, such as current density and faradaic efficiency [4].

Proton Exchange Membranes (PEMs) have continuously been the state-of-the-art of the field, as they are chemically stable membranes that efficiently mitigate product crossover. However, they are relatively expensive and generate an acidic environment on the cathode side, which results in notable hydrogen evolution reaction (HER). PEMs also easily reach an upper threshold in their conductivity due to high polarisation losses and are less effective in hindering the concurrent Hydrogen Evolution Reaction (HER) [2]. On the other hand, anion exchange membranes (AEMs) are the main commercial alternative that addresses the limitations mentioned for PEMs and presents unparalleled

* Corresponding author. Department of Applied Science and Technology (DISAT), Politecnico di Torino, Corso Duca degli Abruzzi, 24, Turin, 10129, Italy.
** Corresponding author.
E-mail addresses: carmelo.parata@polito.it (C. Parata), vasiliki.zogali@advent.energy (V. Zogali).

https://doi.org/10.1016/j.memsci.2026.126301
Received 8 June 2026; Received in revised form 22 September 2026; Accepted 14 October 2026
Available online 16 October 2026
0376-7388/© 2026 The Authors. Published by Elsevier B.V. This is an open access article under the CC BY license (http://creativecommons.org/licenses/by/4.0/).

selectivity and energy efficiency, while being more sensitive to crossover and salt formation, and requiring high alkaline stability to withstand the working conditions [5,6]. Another relevant alternative are bipolar membranes (BPMs), which answer most of the issues from both PEMs and AEMs by utilising an engineered combination of the two [7,8]. However, BPMs are costly and structurally complex which also results in higher ohmic resistances in the device due to increased thickness. Other membrane types like ion-solvating membranes (ISMs) are rapidly becoming a point of interest for various electrochemical applications but are mainly employed in more mature research fields, like water electrolysis, as they require harsh operating conditions such as extremely high concentrated alkaline electrolytes [9].

Many efforts have been devoted to AEM electrolysers, because of the aforementioned advantages and their simplified production processes. Sustainion®, Aemion+®, and PiperION®, are just some of the many commercially available relevant options with attractive properties (Table 1). As anticipated, alkaline stability is one of the main properties required for AEMs, as the setup operates by utilising an alkaline aqueous anolyte. Hydroxide, carbonate, bicarbonate and formate species are the main ion carriers. Due to their strong nucleophilicity and basicity they tend to interact easily with the quaternary ammonium (QA) groups that are chemically tethered on the membrane polymer backbone ultimately causing chemical degradation and loss of membrane ion conductivity. Numerous studies have demonstrated the impact of different combinations of backbones, QA functional groups, and spacers on the performance and durability of such membranes [10–16], with particular interest towards polymers with tunable properties such as polymers with a wide range of degrees of functionalisation (DFs), crosslinked polymers, composites and copolymers [17–21].

It is important to note that different molecular architectures can promote the formation of well-defined microscopic morphologies, which facilitate ion conduction while minimising swelling [25]. Recent studies have consistently shown that hydrocarbon-based backbones are one of the most promising types of polymers for maximising membrane durability [26–28], due to their lack of chemically labile heteroatom linkages, such as aryl ether groups [29]. Within this class, fully aromatic backbones are particularly attractive, combining an interesting set of properties such as low water absorption, high glass transition temperature (T_g), good thermal and mechanical stability [30] and high tunability owing to the numerous available sites for functionalisation.

A key example is the Diels-Alder polyphenylene (DAPP), a polymer with significant thermal and alkaline stability [31]. Each repeating unit is composed of ten highly dense phenylene rings, and its rigid conformation allows for up to six available functionalising sites per repeating unit. DAPP-based polymers functionalised with trimethylammonium (TMA) groups have been synthesised and characterised in previous studies, highlighting the notable alkaline stability of the polymer tethered to TMA *via* a 6-carbon sidechain [32,33]. In this form, the polymer's main degradation pathways are slow Hofmann β-elimination, methyl substitution, and the cross-linking of unreacted alkyl bromides (from the functionalisation intermediate) *via* Br substitution and Williamson ether formation; the latter is most relevant under heterogeneous amination conditions [32]. Stable performance was demonstrated for AEMs employing this backbone functionalised with TMA cationic groups for water electrolysis [34], which also highlighted the relevance of the backbone's mechanical properties that render the membrane easy to handle and transport while maintaining flexibility.

Table 1
Properties of some relevant commercially available AEMs.

AEM	WU (%)	IEC [meq g^{-1}]	σ (80 °C, OH^-) [mS/cm]
Aemion + AF2-HWP8-75-X [22]	56	2.45	>112
Fumasep FAA-3 [22]	55	1.85	70
PiperION [23]	40	2.35	160
Sustainion X37-50 RT[a]	98	1.45	Too swollen to measure at 80 °C [24]

[a] Data for Sustainion X37-50RT was collected experimentally.

Following on these findings, we decided to further investigate DAPP-based AEMs, with the objective of maximising ionic conductivity for the electrochemical CO_2 reduction reaction (CO_2RR) applications while maintaining the high mechanical resistance, stiffness and bendability of DAPP [35] and while improving on the chemical stability in alkaline conditions. Ease of production was prioritised in the development of alternative pathways. In principle, good performance of AEMs needs to be coupled with a cost effective and simple production process for a membrane to achieve commercial relevance. In pursuit of these targets, five families of DAPP-based AEMs were synthesised and characterised, exploring different sidechain carbon length, and post-polymerisation functionalisation pathways.

The *N*-methylpiperidinium group was investigated as the terminal ionic functional QA group replacing TMA. *N*-methylpiperidinium is a cation group that is largely employed in the field of CO_2 electrolysis for its capacity of increasing the transition state energy for the two most common degradation pathways, Hofmann elimination and nucleophilic substitution, due to the conformational restrictions imposed by the ring [36]. Other multi-ringed QAs, such as spirocyclic nitrogen-based QAs, are well known to be able to increase the transition energy further [37,38]. However, in return they sacrifice the capability to achieve a high concentration of ionic carriers due to their high steric hindrance; their synthesis typically requires many complex functionalisation steps often requiring expensive reagents, and their chemical stability significantly outlives other components present in the MEA electrolysers, rendering such high resistance unnecessary. For these reasons, N-methylpiperidinium (N-MePIP) was selected as the QA group in this study, offering a favourable balance between alkaline stability, synthetic accessibility, and achievable conductivity. In parallel, a different sidechain tethering pathway was also attempted, producing sidechains through Friedel-Crafts alkylation, illustrated in Fig. 1 [39]. This approach requires a more streamlined synthetic setup and lower reaction times compared to the previously documented Friedel–Crafts (FC) acylation followed by reduction process and does not require heating. The resulting alkylated sidechains feature a tertiary carbon adjacent to the polymer backbone. This is a result of a mechanistic carbocation rearrangement, causing the formation of a branched methyl group at the linkage site.

To our knowledge, these QADAPP-PIP membranes with such novel molecular structures have not been reported in CO_2 electrolysis. The impact of these structural modifications on various physical and chemical properties, and electrochemical performance was monitored and assessed over the course of the study.

2. Experimental

2.1. Reagents and materials

Dichloromethane (DCM, >99%, LabKem) and chloroform (>99%, LabKem) were dried overnight over molecular sieves (0.4 nm, Merck) before use. N,N-dimethylacetamide (DMAc, 99%, Sigma-Aldrich), trifluoroacetic acid (TFA, 99%, Honeywell), triflic acid (TFSA, 98%, Glentham Life Sciences), 5-bromo-1-pentene (98%, BLD Pharm), 7-bromo-1-heptene (98%, BLD Pharm), 9-bromo-1-nonene (98%, BLD Pharm), aluminium chloride (98%, Sigma- Aldrich), triethylsilane (TES, 99%, Sigma-Aldrich), trimethylamine (TMA, 43-49% in H_2O, Sigma-Aldrich), N-methylpiperidine (N-MePIP, 99%, Sigma-Aldrich), 0.1 M $AgNO_3$ solution (Sigma-Aldrich), diethyl ether (>99%, Sigma-Aldrich), acetone (99.5%, PanReac AppliChem), ethanol (99.8%, PanReac AppliChem), methanol (99.9%, PanReac AppliChem) and N-methyl-2-pyrrolidone (NMP, >99%, Penta) were all used as received. 6-bromohexanoyl chloride (98%, J&H Chem) was purified by vacuum distillation under an inert atmosphere prior to use. The 50 μm filter for

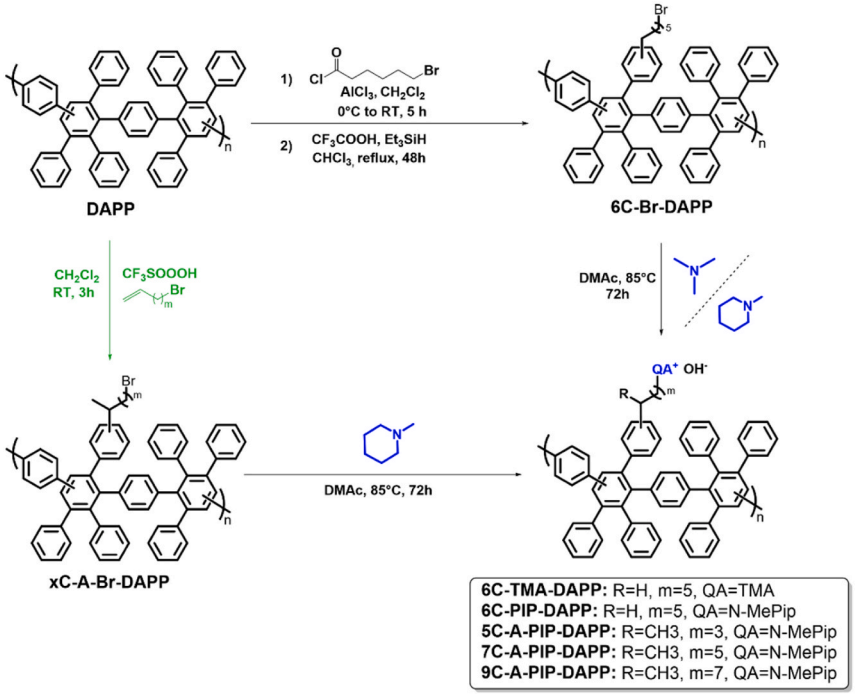


Fig. 1. Synthetic pathways for the functionalisation of DAPP.

membrane fabrication was purchased for Hellenic Filtration Enterprises S.A (HFC).

2.2. Bromoalkylation of DAPP

Diels-Alder Polyphenylene (DAPP) was synthesised using a Diels-Alder (DA) polymerisation, following the procedure detailed in previous literature by Fujimoto et al. [35] with a yield of 99.8% and characterised through Size Exclusion Chromatography (SEC) in $CHCl_3$ ($M_n = 36$ kDa, $M_w = 84$ kDa, $Đ_M = 2.1$). Following polymerisation, the DAPP polymer was post-functionalised using two different pathways to obtain the brominated intermediates 5C-A-Br-DAPP, 6C-Br-DAPP, 7C-A-Br-DAPP, and 9C-A-Br-DAPP as presented in Fig. 1.

For the 6C-Br-DAPP intermediate, a slightly modified procedure from the one reported by Hibbs et al. [33] was followed. The first step is a Friedel-Crafts acylation reaction to introduce sidechains onto the DAPP backbone. The bromo-hexyl sidechains could be attached to any of the six available positions on the pendant aryl groups of DAPP, determining the number of bromohexanoyl moieties per repeat unit and, consequently, the degree of functionalisation (DF). However, due to steric hindrance, polymers with more than four sidechains per repeat unit (DF > 4) were difficult to synthesise. Therefore, the amount of acylating reagent and reaction time were carefully monitored in accordance with the reaction stoichiometry to achieve high DFs. A representative procedure is reported, resulting in a 6C-Br-DAPP with a DF of 3.7, using a 1:5.5 M ratio of DAPP to acylating reagent. Firstly, in a flame-dried 1 L two-neck round-bottom flask equipped with a condenser and a stirrer, DAPP (7.5 g, 9.8 mmol) was dissolved in 460 mL of dry DCM (from a solvent purification system, SPS), kept in molecular sieves overnight) under an inert atmosphere at room temperature. 6-bromohexanoyl chloride (11.6 g, 54 mmol) was subsequently added to the solution. The reaction mixture was cooled down to 0 °C, and $AlCl_3$ (7.23 g, 54 mmol) was added. After complete addition, the reaction was brought to room temperature and left stirring for 5 h. The mixture was concentrated under reduced pressure using a rotary evaporator until approximately half of the solvent volume was evaporated, then precipitated into cold stirred methanol (MeOH) (5x the volume of the reaction solution). The precipitated polymer was filtered, then immersed in MeOH again and stirred for 1 h at 60 °C to remove leftover reagents, filtered again and dried at 80 °C overnight, yielding 11.2 g of the functionalised polymer (81% yield) as a yellowish flaky solid. The intermediate obtained this way was called 6C-O-Br-DAPP and still contains a carbonyl group, which was then reduced to methylene group (-CH_2-) using a large excess of trifluoroacetic acid (TFA) and triethyl silane (Et_3SiH) as the reducing agent, yielding the reduced product of 6C-Alkyl-Br-DAPP. In a flame-dried 1000 mL two-neck, round-bottom flask equipped with a condenser and a stirrer, 6C-O-Br-DAPP (11 g, 7.8 mmol) and 400 mL of $CHCl_3$ (dried overnight over molecular sieves) were added. After complete dissolution of the polymer, 119.7 mL (1911 mmol) of trifluoroacetic acid were added, and then Et_3SiH (40.3 g, 351 mmol) was added dropwise. The reaction was heated under reflux conditions for 24 h. Subsequently, an additional amount of 40.3 g (351 mmol) of Et_3SiH were added dropwise. The reaction was left stirring under reflux for a further 24 h (total reaction time 48 h). The mixture was then left to cool down, poured into an alkaline aqueous solution to neutralise the highly concentrated acid (aq. KOH pH = 8-9, 10x the volume of the reaction volume) and stirred for 1 h. After confirming that the pH was neutralised, a glass separating funnel was utilised to separate the aqueous solution from the organic phase containing the polymer. At this point, the organic phase was precipitated in MeOH. The MeOH was filtrated to obtain the polymer, which was redispersed in MeOH, and stirred for 1 h at 60 °C, filtrated again and dried overnight at 80 °C under vacuum. 10.1 g of product were obtained (95% yield) as a yellowish solid. Complete reduction was confirmed by ^{1}H NMR spectroscopy, which was also utilised to confirm the degree of functionalisation of the polymer.

A different one-step super-acid-catalysed Friedel-Crafts bromoalkylation process was employed to obtain 5C-A-Br-DAPP, 7C-A-Br-DAPP and 9C-A-Br-DAPP [39]. Alkene-terminated bromoalkyl reagents were employed instead of the alkyl chlorides used in the first process to enable the efficient introduction of bromoalkyl groups onto the aromatic rings of polymers. After extensive optimisation of the reaction conditions to obtain a DF > 3.5, an excess of both the alkene and triflic acid was used, with a molar ratio of 1:6 relative to the repeating units of the DAPP backbone polymer. The resulting side-chain structural variances were based on the corresponding alkene reagent (5-bromo-1-pentene,

7-bromo-1-heptene, 9-bromo-1-nonene). A representative procedure for 7C-A-Br-DAPP is described as follows: in a flame-dried 500 mL two-neck, round-bottom flask equipped with a condenser and a stirrer, DAPP (4 g, 5.3 mmol) and 7-bromo-1-heptene (5.59 g, 31.5 mmol) were dissolved in 210 mL of dry DCM at room temperature. The reaction mixture was cooled down to 0 °C using an ice bath, and 2.73 mL (31.5 mmol) of TFSA were added dropwise. Upon the addition, the colour of the reaction turned black immediately and its viscosity increased. The reaction was then left stirring at room temperature for 3 h, then precipitated in MeOH, filtrated and immersed in fresh MeOH again at 60 °C for 1 h. The final product was filtered and dried overnight at 80 °C under vacuum, obtaining the polymer in the form of a yellowish powder (6.2 g, 82% yield).

2.3. Functionalisation with QA cations

The process of homogeneous amination was carried out using the same general procedure on all the brominated intermediates, employing either TMA or N-MePIP as nucleophiles to tether the two different cationic groups. The reaction followed the widely applied Menshutkin-type nucleophilic substitution of the terminal alkyl bromide by the tertiary amine. A representative procedure of tethering of N-MePIP on 6C-Br-DAPP (with a DF of 3.7) is reported as follows: in a 500 mL one-neck, round-bottom flask equipped with a condenser and a stirrer, 6C-Br-DAPP (5 g, 3.6 mmol) was dissolved in 160 mL of NMP at room temperature. N-MePIP (5.34 g, 53.9 mmol, 4 equivalents relative to cationic groups) was added to the mixture dropwise. The reaction flask was then heated to 85 °C and stirred for 4 days. At the end of the reaction, the solution had darkened but remained homogeneous and no gel formation was observed. The resulting solution was precipitated in diethyl ether and washed multiple times with fresh diethyl ether. The product of 6C-PIP-DAPP (5 g, 95% yield) was obtained as a dark orange powder and dried under vacuum overnight at 80 °C. All the other final derivatives of the QA polymers, 6C-TMA-DAPP, 5C-A-PIP-DAPP, 7C-A-PIP-DAPP and 9C-A-PIP-DAPP were synthesised using this general procedure and appeared as dark orange powders.

2.4. Structural characterization

The polymers were structurally characterized *via* ^{1}H NMR spectroscopy. Spectra were recorded at 600 MHz using CD_2Cl_2, $CDCl_3$ and DMSO-d_6 as solvents. The molecular weight and dispersity index ($Đ_M$) of the DAPP backbone were determined by size exclusion chromatography (SEC) in $CHCl_3$, utilising an Agilent system equipped with an Agilent PLgel MIXED guard column (7.5 × 50 mm, 5 μm) and an Agilent PLgel MIXED-C column (300 × 7.5 mm, 5 μm).

2.5. Membrane preparation

1 g of each cationic polymer was dissolved in 6 mL DMAc to obtain a 17% wt.% solution, stirred and heated to 40 °C to form a homogeneous solution. The solution was then filtered using a 50 μm filter, supplied from HFC, to remove impurities and aggregations. It was then manually cast onto a heated (50 °C) HDPE substrate using a doctor blade coater set to a gap height of 500 μm and moving horizontally at a rate of 3 mm/s. After casting, the newly formed AEM was left to dry on the heated surface for 1 h and then transferred to a vacuum oven to be dried at 80 °C overnight. The membrane was then washed in hot water (60 °C) for 5 h to remove residual DMAc and other impurities, followed by a second drying step at 80 °C overnight. Lastly, it was cut into 10 × 10 cm pieces and stored under humid conditions. To convert the membranes to the hydroxide (OH^-) form, the AEMs were immersed in 1 M aqueous NaOH overnight. The resulting AEMs had an average thickness of 40 μm.

2.6. IEC, water uptake and swelling ratio calculation

The IEC of the polymers was spectroscopically evaluated utilising the formula:

$$IEC_{Th} = \frac{DF \times 1000}{M_{R,(OH-form)}}$$

The IEC was also experimentally evaluated by utilising a Mohr titrator (Eco Titrator, Metrohm). The samples (30-40 mg) were dried overnight at 60 °C, then immersed in a 0.5 M aqueous HBr solution for 5 h to obtain the polymer in the Br^- form. The samples were subsequently washed multiple times with deionised water until the pH of the bath reached neutral pH. Afterwards, the samples were immersed in 0.1 M $NaNO_3$ aqueous solution (35 mL) for 48 h to complete ion exchange. The titration was then performed utilising a 0.1 M $AgNO_3$ aqueous solution. Each type of membrane was tested multiple times to ensure reproducibility. The values of IEC in Br^- form were calculated by the device utilising the formula:

$$IEC_{titr,Br} = \frac{C_{AgNO_3} \times V_{AgNO_3}}{w_{dry(Br-form)}}$$

where C_{AgNO3} and V_{AgNO3} are, respectively, the concentration and the volume of $AgNO_3$. These values were then converted into OH^- form by utilising the formula.

$$IEC_{titr,OH} = \frac{IEC_{Br}}{1 - \frac{IEC_{Br} \times (M_{Br^-} - M_{OH^-})}{1000}}$$

For the water uptake (WU) and swelling ratio (SR) measurements, some samples of the Br^- form membranes were dried overnight in the oven at 80 °C under vacuum. They were then cut into 2.5 × 2.5 cm^2 squares and weighed in their dry form. After that they were stored in deionised water for 24 h. The excess surface water was gently removed with a lint-free tissue before measuring the membrane wet weight and the swollen dimensions of its sides. Each measurement was taken on a minimum of 3 different samples per type of polymer. The values of WU% and SR% were then calculated using the formula:

$$WU\% = \frac{W_{wet} - W_{dry}}{W_{dry}} \times 100$$

$$SR\% = \frac{L_{wet} - L_{dry}}{L_{dry}} \times 100$$

The number of H_2O molecules around each QA group is defined as hydration number (λ), was calculated using the formula:

$$\lambda = \frac{WU(\%) \times 10}{IEC_{titr,OH} \times 18}$$

2.7. Ion conductivity measurement

Ion conductivity (σ, mS/cm) was evaluated for each membrane in OH^- form utilising a 4-point probe method in a BT-112 Conductivity Cell setup (Scribner). Membranes were cut to a size of 3 cm × 1 cm and dipped in 1 M KOH aq. solution for 1 h to ensure full exchange. Measurements were performed under fully hydrated conditions at 80 °C while the cell was fully immersed in deionised water. The cell was kept in the setup for 45 min under stable conditions before performing electrochemical impedance spectroscopy (EIS) measurement for each membrane sample with an Autolab PGSTAT302 potentiostat equipped with a current booster. EIS tests were performed in the frequency range 1 MHz-10 Hz, using a voltage of 0.8 V with a signal amplitude of 80 mV. Ionic conductivity was calculated using the formula:

$$\sigma = \frac{L}{R \times W \times T}$$

where L is the distance between the two inner platinum wires (0.425 cm), R is the resistance of the membrane in Ohm obtained from the EIS measurement, and W and T are the width and thickness of the membrane, respectively.

2.8. Thermal characterisation

To investigate the thermal decomposition of the polymers, Thermogravimetric analysis (TGA, Linseis GmbH, Europe) was carried out on polymers in their powder form. Before the characterisation, the powder samples were annealed for 30 min in a vacuum oven to 110 °C to remove any volatiles. TGA was then run under N_2 atmosphere from 20 °C to 600 °C utilising a constant ramp of 5 °C/min. From this test, the shape of the degradation curve and the values of $T_{d,95\%}$ were obtained.

2.9. Small-angle X-ray scattering (SAXS) measurements

SAXS curves were acquired using a Malvern PANalytical Empyrean diffractometer with a CuK(α) radiation (λ = 1.54 Å) and operating at 40 kV and 45 mA. For each of the five different polymeric membranes, measurements were carried out on multiple samples to have reliable results. 1D-SAXS measurements were carried out in transmission geometry out in a vacuum path chamber (Scatter X78) with a beam with line collimator and a GaliPIX3D detector. The membranes in the dry form were cut into a standardised size of 0.5 × 2 cm^2 and placed in an aluminium sample holder. Scans were performed in the q region 0.1-3.5 nm^{-1}, by using a step size of 0.014° and an exposure time of 30 min. Data analysis was carried out with the EasySAXS software (Malvern-PANalytical).

The scattering vector (q) is defined and obtained as:

$$q = \frac{4\pi}{\lambda \times \sin(2\theta)}$$

where λ is the wavelength of the CuK(α) radiation, and 2θ is the total angle between the incident beam and the detector. From the value of q, the average distance between ionic clusters (d) was easily calculated as:

$$d = \frac{2\pi}{q}$$

2.10. Evaluation of alkaline stability

The alkaline stability of the membranes was evaluated by comparing the ^{1}H NMR spectra of samples before and after a degradation test. This method has been utilised by previous studies with varying testing conditions [40]. Samples of the pristine membranes were diluted in DMSO-d_6 and analysed by ^{1}H NMR spectroscopy. These spectra were compared to the ones of the membranes after the test in alkaline media. The test was performed by immersing the membrane pieces in a 1 M NaOH aqueous solution at 90 °C for 125 h and 250 h. The samples were then washed multiple times with deionised H_2O to remove any excess ions and until neutral pH, diluted in DMSO-d_6 and used for ^{1}H NMR spectroscopy characterisation. Complementary data on the alkaline stability was also collected by evaluating the retained OH^- conductivity and retained IEC after the test in alkaline media.

2.11. MEA in-operando characterisation

The performance of the membranes was evaluated in a gold plated MEA cell (Fuel Cell Store) operating for CO_2RR. The cell had a 5 cm^2 active area. A carbon paper gas diffusion layer (GDL, SIGRACET 28BC, Ion power GmbH) was sputtered with Ag utilising a magnetron sputtering device (Quorum Technologies Ltd., Q150T S) at 50 mA for 900 s to act as the cathode. The deposition was carried out until obtaining around 0.7 mg/cm^2 of Ag. A commercial Ti mesh coated with IrO_2 (purchased from Shouyiji Trade Xiamen and used as received) was utilised as the anode. Sustainion ® X37-50 Grade RT was utilised as a comparative commercial membrane. A picture of the setup with detailed layers is reported in Fig. S1. Electrochemical tests on the cell were performed using a potentiostat (BioLogic SP 300) equipped with a current booster (10 A). 0.5 L of a 0.1 M aqueous $KHCO_3$ solution was utilised as anolyte and recirculated during the tests at a rate of 20 mL min^{-1}, utilising a peristaltic pump. Dry CO_2 (30 sccm) was fluxed to the cathode side utilising a mass flow controller. Chronopotentiometry (CP) was performed at current densities of 100 and 200 mA cm^{-2}. Chronoamperometry (CA) was performed at cell voltages of 3.2 V and 3.7 V. Linear sweep voltammetry was carried out in the range between 0 V and 4 V utilising a scan rate of 25 mV s^{-1}. EIS was carried out in the frequency range 1 MHz-10Hz, during operation at 1.5, 2.5 and 3.2 V. HPLC (Nexera series, SHIMADZU) was used to detect and quantify the liquid products that crossed over to the anolyte. A sample of the recirculated anolyte was collected at the end of each run to confirm the presence of liquid products (specifically formic acid and ethanol) for the faradaic efficiency (FE) total calculation. A micro gas chromatograph (GC, Fusion®, INFICON) was utilised in line to analyse the gaseous products. The GC is composed of two channels with a 10 m Rt-Molsieve 5 A column and an 8 m Rt-Q-Bond column, both equipped with a micro thermal conductivity detector. Ar and He were used as carrier gases for the Molsieve 5 A and Rt-Q-Bond columns respectively, to evaluate H_2 and CO in the first column and CO_2 in the second column. From the measured concentration of products, FE was calculated using the formula:

$$FE(\%) = \frac{n \times N \times F}{Q} \times 100$$

where n is the number of electrons required to form one molecule of product, N is the measured number of moles of the product, F is the Faraday constant and Q is the charge consumed over the considered period. The gas selectivity (%) of each product was then calculated as:

$$Select_x = \frac{FE_x}{FE_{GasTOT}}$$

In AEMs, the transport of charge happens through multiple species. Transport species originated from cathodic CO_2 (CO_3^{2-}, HCO_3^- and $HCOO^-$) cause CO_2 crossover and release in the anode compartment. During the chronopotentiometry runs, some gas chromatography data of the anodic gaseous output was collected to assess the prevalent charge transporting species in our membranes at both monitored current densities. This assessment was done by comparing the expected theoretical values of the ratio for each ion, to the ones obtained from the experiments.

3. Results and discussion

3.1. Membranes synthesis and morphology (SAXS)

The DAPP polymer was synthesised according to previous literature [35]. The dispersity and M_w of the polymer could be tuned by changing the reaction conditions and time. DAPP was synthesised with a total yield of 88%, including the monomer synthesis, and characterised through SEC in $CHCl_3$. The batch selected as the starting material for functionalisation has a M_w of 84 kDa and a $Đ_M$ of 2.1. The functionalisation pathways of the polymer are shown in Fig. 1.

In particular, two synthetic pathways were employed to obtain the brominated intermediates. The first involves a FC acylation followed by a reduction step to obtain the linear sidechain. In this pathway 6-bromohexanoyl chloride is tethered to the polymer backbone, and the resulting ketone is subsequently reduced to a methylene group. The second route utilises direct super-acid-catalysed FC alkylation to obtain the branched sidechains, containing a tertiary carbon adjacent to the polymer

backbone. The resulting intermediates were subsequently quaternised *via* homogeneous amination with the two employed cationic groups (TMA or N-Methyl piperidine) to obtain polymer powders that were soluble in DMSO for characterisation and DMAc for membrane casting. A solution of each polymer in DMAc was blade-cast into membranes with an average thickness of 40 μm. The chemical structures and the purity of the reaction intermediates and final products were confirmed by ^{1}H NMR spectroscopy (Fig. S2). The purity of all obtained products was higher than 99%, confirming the high selectivity of the selected post-functionalisation processes. The number of cationic groups per repeating unit varied depending on the reagent stoichiometry used during the functionalisation reactions.

Each polymer presented a different limiting DF, as steric hindrance can prevent certain sites from reacting, even in the presence of reagent excess. For each product, using a fixed stoichiometric ratio of approximately 1:6 between the DAPP polymer backbone and the alkylation reagent, the resulting DFs ranged from 3.5 to 4.4.

Structural characterisation was performed *via* SAXS, to study structure formation (Fig. 2, Fig. S3). Clear ionomer peaks (i.e., local maxima of the scattering curves in the low q region) [41] at $q_{max} \sim 1.67$ nm^{-1} were observed for 9C-A-PIP-DAPP, corresponding to a characteristic ionic cluster distance d = 3.76 nm, as reported in Table 2. This is the highest *d* value amongst the characterised polymers, which is coherent with the combination of low DF and long spacer chains. 7C-A-PIP-DAPP also shows a clear ionomer peak around $q_{max} \sim 2.06$ nm^{-1} corresponding to characteristic distance of d = 3.06 nm, which is lower compared to 9C-A-PIP-DAPP, as it possesses higher group density and shorter

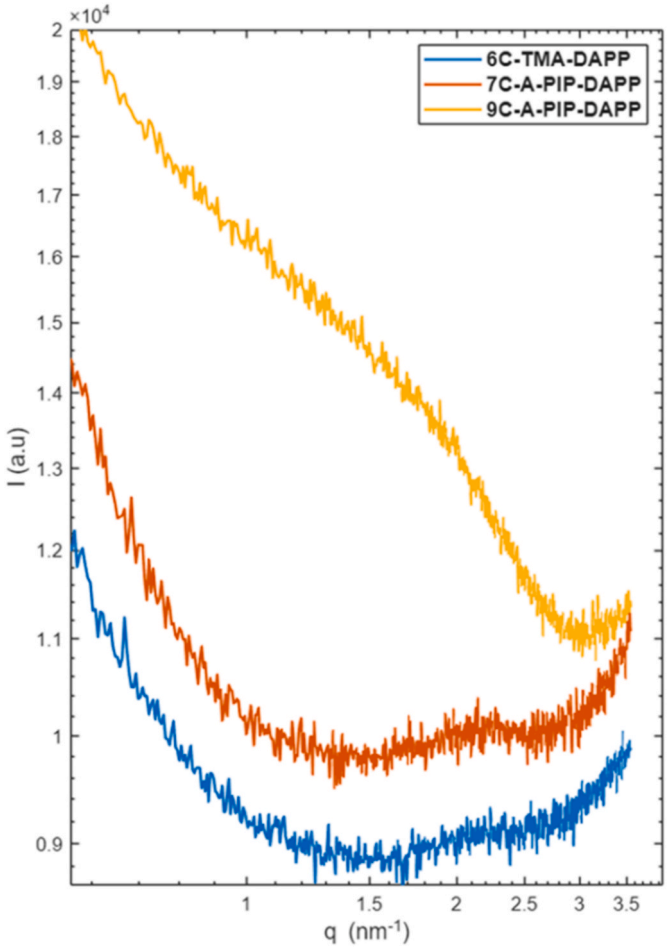


Fig. 2. SAXS profiles of dry AEMs in the range 0-3.5 q for the three membranes showing clear peaks (6C-TMA-DAPP, 7C-A-PIP-DAPP and 9C-A-PIP-DAPP). The data was measured with AEMs in Br^- form and shifted vertically for clarity.

Table 2
AEMs scattering vectors (q) and distance between ionic clusters (d), derived from SAXS.

AEM	q [nm^{-1}]	d [nm]
6C-TMA-DAPP	2.14	2.94
6C-PIP-DAPP	-	-
5C-A-PIP-DAPP	-	-
7C-A-PIP-DAPP	2.06	3.06
9C-A-PIP-DAPP	1.67	3.76

sidechains. The trend is confirmed by 6C-TMA-DAPP, with a peak around $q_{max} \sim 2.14$ nm^{-1} corresponding to d = 2.94 nm. This polymer has lower cation group density, but a linear sidechain structure and smaller cationic groups. Finally, no ionomer peaks were observed for 5C-A-PIP-DAPP and 6C-PIP-DAPP. This is possibly because of the much shorter inter-ionic distance originating from a combination of high group density, shorter sidechain lengths and, for the case of 6C-PIP--DAPP, linear sidechain structure. This possibly prevented the formation of a distinct morphology on the nm level [42].

3.2. IEC, water uptake and hydroxide conductivity

The values of water uptake, swelling ratio and IEC derived both by NMR and by Mohr titration are reported in Table 3. All the IEC values measured *via* Mohr titration were lower than the ones derived from NMR, corresponding to 90-95% of the theoretical values, in accordance with previous works on AEMs [10]. Shorter sidechains were tethered at higher densities on this backbone, reaching a DF of up to 4.5 for 5C-A-PIP-DAPP due to reduced steric hindrance. Alkylation reactions generally yielded higher DFs at comparable spacer lengths, as can be observed by the data for 6C-TMA-DAPP, 6C-PIP-DAPP, and 7C-A-PIP--DAPP. Among the polymers studied, 5C-A-PIP-DAPP clearly showed the highest IEC value due to its combination of low repeat-unit M_w and high cationic group density. Despite possessing similar sidechain lengths, 7C-A-PIP-DAPP, 6C-PIP-DAPP and 6C-TMA-DAPP had different DFs, varying in a range from 3.5 to 4.2; nonetheless, differences in repeat-unit M_w result in comparable IEC values for these polymers. As expected, 9C-PIP-DAPP had the lowest IEC, consistent with its high repeat-unit M_w and average DF. All polymers showed low swelling ratios at room temperature, not significantly influenced by the variations in side-chain chemistry or size. Water uptake at room temperature showed more pronounced differences, which can be well-correlated with both the IEC values and the morphology of the polymer [43]. Water uptake values are closely associated with potential MEA flooding, as excess water transported to the cathode side can diffuse into the cathodic chamber. Thus, an optimal balance is required: the polymer should possess a water uptake high enough to generate well-developed hydrophilic domains that facilitate ion transport, but not excessively high as it could negatively impact the performance at higher current densities [44]. Usually, polymers exhibiting poor clustering and structural order are associated with higher WU values [45], as amorphous regions tend to be more hydrophilic. This structural feature results in WU% values above 60% for all the polymers studied. Among them, 5C-A-PIP-DAPP shows the highest WU (95%), which is coherent with the highly amorphous morphology observed by SAXS results. In general, WU decreases for polymers with lower IEC values [21]. However, the behaviour of 6C-PIP-DAPP deviates from this trend, as it shows similar IEC to 6C-TMA-DAPP and absence of SAXS peaks but still has the lowest WU (68%) among the investigated membranes.

The hydration number in OH^- form was calculated for the samples, showing values in a range between 15 and 21. Overall, these values are average when compared to other AEMs [15,46,47].

Table 3
Properties of the AEMs.

AEM	DF[a]	IEC_{NMR}[b] [meq g^{-1}]	IEC_{titr}[b] [meq g^{-1}]	$T_{d,95}$[c] [°C]	Water Uptake (%)	λ (OH^-)	σ (80 °C, OH^-) [mS/cm]	Swelling Ratio (%)
6C-TMA-DAPP	3.5	2.50	2.29	210	85	18.1	126	12
6C-PIP-DAPP	3.7	2.44	2.25	226	68	16.8	133	12
5C-A-PIP-DAPP	4.4	2.69	2.47	228	95	20.7	122	16
7C-A-PIP-DAPP	4.1	2.43	2.31	226	81	19.5	117	12
9C-A-PIP-DAPP	3.8	2.29	2.15	223	75	19.4	108	12

[a] Degree of functionalisation calculated as the average amount of sidechains per repeating unit.
[b] Values in hydroxide form.
[c] Measured by TGA.

3.3. Ionic conductivity

The ionic conductivity values of all the AEMs were measured at 80 °C in deionised water and are reported in Table 3. The values of conductivity for the polymers with the branched sidechains are increasing for shorter sidechains and proportionally to the IEC. 9C-A-PIP-DAPP has the lowest conductivity with a value of 108 mS cm^{-1}, while 7C-A-PIP-DAPP shows a conductivity of 117 mS cm^{-1} and 5C-A-PIP-DAPP is at 122 mS cm^{-1}. The two polymers with linear spacers showed the highest conductivities, with respective values of 126 mS cm^{-1} for 6C-TMA-DAPP and 133 mS cm^{-1} for 6C-PIP-DAPP. Values of OH^- above 100 mS/cm at 80 °C are desirable, and this requisite is met by all the DAPP membranes we characterised, with the highest conductivities reaching quite interesting values.

3.4. Thermal properties

Thermal stability was studied *via* TGA under a nitrogen atmosphere after pre-drying the samples at 110 °C to remove volatiles. The temperatures corresponding to 95% mass retention, $T_{d,95\%}$, are recorded in Table 3 and the compared TGA curves are shown in Fig. 3. All the polymers exhibited a two-step degradation profile. The first step is attributed to the decomposition of the sidechains and QAs, while the second one is due to decomposition of the polymer backbone. All the PIP-functionalised polymers have similar $T_{d,95\%}$ around 226 °C, whereas the TMA-functionalised polymer showed a slightly lower average value of 210 °C. These results indicate that the spacer length does not have a relevant impact on the thermal stability of these polymers, while it is only slightly impacted by the nature of the cationic group. The second step of the decomposition, occurring at approximately 390 °C, is the same for all the five polymers, since it corresponds to backbone decomposition. The relative mass change at 600 °C is reasonably higher for polymers with higher DFs, reflecting the larger contribution of the sidechains to the total polymer mass.

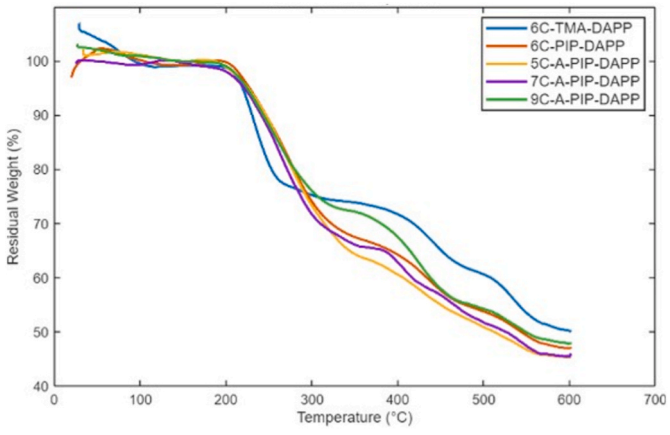


Fig. 3. TGA profiles for all the polymers, measured under N_2 with a 5°/min temperature ramp.

3.5. Alkaline stability

Polymer degradation was evaluated by ^{1}H NMR spectroscopy, to investigate the stability of the DAPP polymers under harsh alkaline environment (1 M NaOH, 90 °C under argon atmosphere). These conditions are significantly more severe than the typical device-operating conditions (room temperature with 0.1 M $KHCO_3$ aqueous anolyte) and were therefore used to accelerate and outline potential degradation processes. Membrane samples were collected after 125 h and 250 h of exposure. Complementary comparative data on each membrane's retained IEC and conductivity values were also gathered after the longest stability tests (Table 4). The 6C-PIP-DAPP sample remained stable throughout the test and until 250 h without significant degradation. As shown in Fig. 4, the spectra of the polymers largely overlap over time, although there is an evident separation between certain polymer peaks and the water signal is observed in some of the spectra, likely depending on the water content in the NMR solvent. Additionally, a gradual sharpening of the peak at 1.2 ppm is observed during the test. This peak is not associated with known degradation pathways, and it is likely related to slight peak shifting associated with counterion exchange or changes in solvation, rather than chemical degradation. This reflected in the retained IEC and conductivity values, which were substantially 99-100% of the original values.

By contrast, 6C-TMA-DAPP showed a loss of solubility in DMSO-d_6 and DCM-d^2 after 125 h under the alkaline testing conditions. This can be associated with S_N2 substitution at the trimethylammonium group, combined with partial crosslinking of the unconverted terminal alkyl bromide sites. Such degradation pathways for the 6C-TMA-DAPP polymer have been previously proposed by Park et al., who also described their possible mechanisms [32], occurring under high-temperature alkaline conditions. Given the insolubility, the evaluation of retained IEC and conductivity are particularly significant for the quantification of the degradation effect on this polymer: we can observe a conductivity retention of only 69%, and IEC retention of 85%. This confirms that polymers functionalised with two different QAs groups, despite having the same spacer length, follow different degradation pathways and kinetics on this DAPP backbone.

The three polymers with methyl-branched sidechain polymers showed more pronounced degradation. New ^{1}H NMR peaks appeared at 4.9 and 5.7 ppm, commonly associated with vinyl groups, along with several additional signals in the alkane region, including a sharp peak around 2.2 ppm. Similar degradation patterns have been observed in previous literature [40,48]. The alkene peaks are usually associated with

Table 4
Retained IEC and σ values for each membrane type after 250 h in 1 M NaOH at 90 °C.

AEM	Retained IEC	Retained σ (80 °C, OH^-)
6C-TMA-DAPP	85%	69%
6C-PIP-DAPP	100%	99.5%
5C-A-PIP-DAPP	83%	72%
7C-A-PIP-DAPP	96%	89%
9C-A-PIP-DAPP	96%	87%

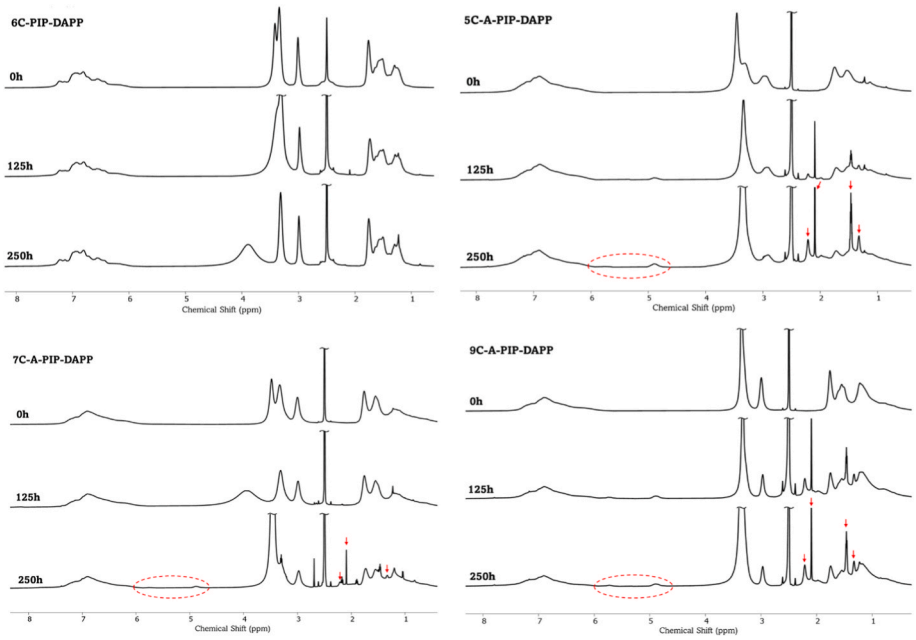


Fig. 4. ^{1}H NMR spectra of DAPP functionalised with 6C-PIP, 5C-A-PIP, 7C-A-PIP and 9C-A-PIP after storage in 1 M aq. NaOH for 0h, 125h and 250h, respectively. The peaks associated to vinyl groups are circled in red, while the peaks originating from structural rearrangement of the sidechain are identified with red arrows pointing at them. (For interpretation of the references to colour in this figure legend, the reader is referred to the Web version of this article.)

the formation of a vinyl group [-CH═CH_2] *via* degradation by β-Hoffman elimination. The rest of the newly formed peaks originate from the structural rearrangement of the sidechain following elimination. This degradation is less evident for the 7-chain derivative, which nevertheless showed some loss of solubility, and more evident for 5C and 9C. Novel peaks are barely present after 125 h and are more prominent after 250 h.

The retained IEC and conductivity measurements are helpful in quantifying which of the branched polymers seem to suffer the most from the permanence in alkaline media. Specifically, 5C-A-PIP-DAPP shows by far the most significant loss of conductivity (72% retained conductivity and 83% retained IEC), compared to respectively 89% and 87% for its 7C and 9C equivalents (both retaining 96% of their IEC). This confirms that the shorter sidechain is the most active towards β-Hoffman elimination due to the higher reactivity of the β hydrogen. The relevance of the sidechain length and structure on the half-life of QA-containing polymers has been highlighted by previous research [49], stating that sidechains of optimal length can suppress and limit elimination, while half-life was shown to quickly drop outside of the optimal area. In the present study, the alkylated sidechains contain a methyl group on the tertiary carbon adjacent to the backbone, leading to a different optimal length and lowering overall stability. These sidechains seem to provide suboptimal protection against β-elimination, and especially in the case of the shortest 5C sidechain. This is realistically related to the presence of one extra site for degradation: the β-carbon relative to the methyl group [50]. Overall, the linear sidechains of 6C-PIP-DAPP polymer exhibit better alkaline stability than the others with TMA or methyl-branched side chains, as they provide adequate distance from the backbone, reduce the number of reactive β-carbons, and promote QA sufficient shielding against nucleophilic attack and S_N2 degradation.

3.6. MEA cell performance

The membranes were tested utilising an MEA cell. The same setup was also tested with the same conditions employing Sustainion® X37-50 RT, as a benchmark against a relevant commercially available option [51,52]. All the tested membranes had a wet thickness of around 40 μm.

The quantification of the anodic side gases highlighted a similar trend for all the membranes (Fig. S4), showing that at each monitored current density the anodic CO_2/O_2 ratio is around a value of 2. This is the expected ratio value if the transport was carried out entirely through CO_3^{2-} ions [53], but it is important to note that, since ionic transport in CO_2RR involves the simultaneous participation of multiple species, this ratio can much more likely originate as an average value of the ratios of all the involved ions (OH^-, CO_3^{2-}, HCO_3^-). Regardless, it is relevant to observe that all the characterised polymers present the same trend for this ratio, confirming the similar nature of the transport mechanism happening in each of them.

The polymer membranes bearing the linear-side chains (6C-TMA-DAPP and 6C-PIP-DAPP) show consistent LSV profiles with an exponential trend, reaching values of 280 mA cm^{-2} and 340 mA cm^{-2} at 4 V, respectively (Fig. 5). This compares well with the Sustainion® membrane, which reached values close to 300 mA cm^{-2}. For the CP, both the membranes showed stable operating conditions at 100 mA cm^{-2} (Fig. S5) and, for up to 20 h, at 200 mA cm^{-2} (Fig. S6). At 100 mA cm^{-2}, 6C-TMA-DAPP showed an average voltage of 3.4 V, while 6C-PIP-DAPP showed an average voltage of 3.2 V, comparable to the one of the setups

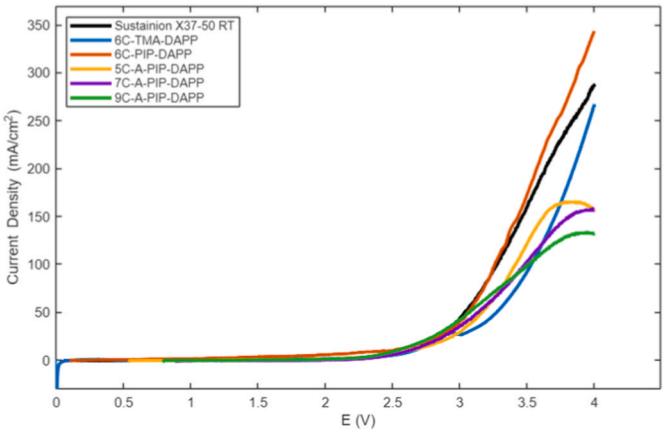


Fig. 5. Linear Sweep Voltammetry tests performed on the setups in operating conditions, performed after the longest operation time achieved for each type.

employing Sustainion® X37-50 RT (3.15 V, Fig. 6a and Fig. S5). The presence of the PIP group thus translates into a good performance improvement, possibly due to better ionic pathways and lower water uptake. At this current density, the gaseous product selectivity is around 99% towards CO and 1% towards H_2 for both 6C-TMA-DAPP and 6C-PIP-DAPP. Gaseous products make up 90% of the total FE, with the liquid formic acid making up the rest (Fig. 6c). This is the expected result with optimal performance, as the employed cathode (sputtered Ag) is well known for its high selectivity towards CO production. The selectivity compares well with the cell employing Sustainion® X37-50 RT in the same conditions, proving that at this current density the DAPP polymers with the linear sidechains can be valid solutions. At 200 mA cm^{-2}, 6C-TMA-DAPP operated at an average voltage of 3.7 V for 20 h (Fig. S6). Around that time, the voltage started decreasing linearly in correspondence with a decrease in monitored flow on the gas outlet. It is reasonable to assume that this behaviour is caused by excessive salt formation on the cathode side of the cell, limiting the cathodic active area and partially blocking the pathway for CO_2, causing an overpressure in the system (Fig. S7). The gaseous product selectivity shifted gradually from the first hours of operation (in which high CO selectivity was observed, Fig. 6d) and stabilised after few hours around 40% CO and 60% H_2. The same trend was observed for Sustainion® X37-50 RT in these operating conditions (Fig. S6). Operational voltage for 6C-TMA-DAPP at 200 mA cm^{-2} is also comparable to the setups employing Sustainion® X37-50 RT, showing that this polymer's performance scales more effectively at higher current densities. Comparatively, 6C-PIP-DAPP at 200 mA cm^{-2} showed an average operating voltage of 3.6 V for up to 20 h (Fig. 6a), slightly lower than both Sustainion® X37-50 RT and 6C-TMA-DAPP yet still demonstrating relative improvement at higher current densities. In this case, there was a slower deposition of salt on the cathode side compared to 6C-TMA-DAPP (Fig. S7), and consequently there was no gradual decrease observed in flow and voltage (Fig. S6). This behaviour is likely related to the lower WU of this membrane, which ends up being an advantage for this application given the working conditions. Minor voltage drops were observed during the overnight tests, which can originate from brief anolyte recirculation irregularities and from the (bi)carbonate formation and dissolution [54]; after each drop the stable voltage was promptly recovered. During the 20-h tests, the gaseous product selectivity shifted gradually from the first hours of operation (in which high CO selectivity was observed) and stabilised after few hours at approximately 40% CO and 60% H_2, in line with the behaviour of 6C-TMA-DAPP and Sustainion® X37-50 RT. In these specific operation conditions, the overtime transition to a more prominent HER is likely caused by the precipitation of salts on the surface of the cathode, reducing the CO_2 availability on the surface and instead favouring the hydrogen evolution reaction. This is coherent with previous studies [55]. The FE towards gaseous products is also comparable, closing at nearly 90% with the rest of the product being liquid formic acid (Fig. 6c). For the 6C-PIP-DAPP, deemed the most interesting of the bunch, a longer test at 200 mA/cm^2 with optimised conditions was carried out to gain further insight into the qualities of the membrane (Fig. S8). In this test, performed with the same cell components and parameters, the anolyte was replaced frequently, and a high gaseous pressure was periodically forced on the cathode side to limit the impact of salt formation. The test showed great performance stability for more than 60 h and highlighted that a high gaseous product selectivity towards CO (80-90% throughout the test) can be maintained for a notably longer period by limiting the salt formation, confirming that the membrane does not lose its selectivity.

Notably, setups employing Sustainion® X37-50 RT would often incur in pinhole formation and structural degradation within 15-20 h of operation, leading to product crossover and the subsequent loss of effective performance. In contrast, this issue was not observed in either 6C-TMA-DAPP or 6C-PIP-DAPP membranes, which demonstrated superior mechanical stability and were more durable towards this type of structural damage, exhibiting the possibility to be recovered after a run (Fig. S9).

The alkylated-sidechain-membranes (5C-A-PIP-DAPP, 7C-A-PIP-

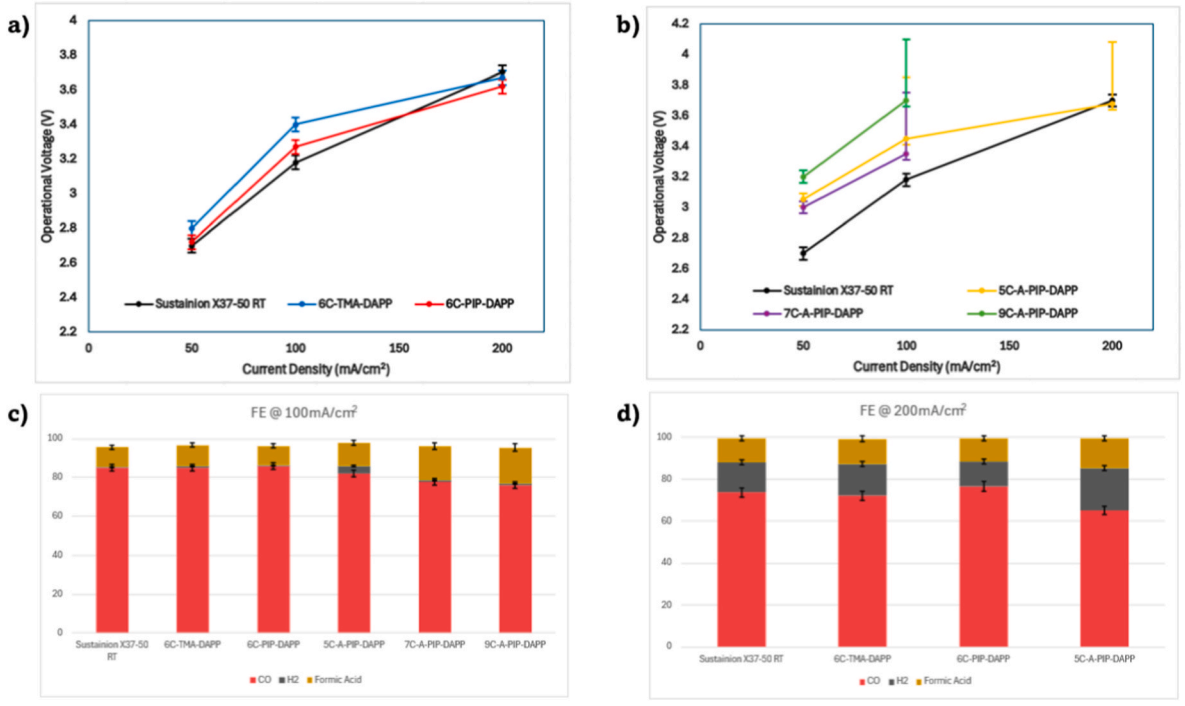


Fig. 6. a) Operational voltage for the acylated + reduced sidechain polymer membranes, compared with Sustainion® X37-50 RT in the range 50-200 mA/cm^2 b) Operational voltage for the alkylated sidechain polymer membranes, compared with Sustainion® X37-50 RT in the range 50-200 mA/cm^2 c) Faradaic Efficiency for all the membranes at 100 mA/cm^2, evaluated over the course of the first 40 min of operation. d) Faradaic Efficiency for the setups employing the four membranes that could withstand testing conditions of 200 mA/cm^2: Sustainion® X37-50 RT, 6C-TMA-DAPP, 6C-PIP-DAPP and 5C-A-PIP-DAPP. Evaluated over the course of the first 40 min of operation.

DAPP, 9C-A-PIP-DAPP) showed distinct behaviour. Prior to chronopotentiometry testing, all three membranes showed low current densities at voltages up to 4 V (determined *via* LSV). In accordance with this, starting a CP measurement directly at 100 mA cm^{-2} would often result in tension above 5 V, triggering automatic shutdown due to safety limits. For this reason, a current ramp protocol was needed to reach operational current densities: the CP was initially set to 20 mA cm^{-2}, then increased by 20 mA cm^{-2} every 3 min until reaching the desired conditions (100 mA cm^{-2} or 200 mA cm^{-2}). This approach enabled operation at the target currents. The LSV of the alkylated membranes performed after the CP ramp shows that these can reach much higher values of current densities when compared to the LSV before operation (Fig. S10). This could be associated with the initial difficulty in forming efficient ionic channels for anion transport, answered by utilising a ramp to reach operational voltages.

The electrolyser incorporating 9C-PIP-DAPP could not be stably operated at 200 mA/cm^2 without spiking above 5 V tension despite the ramp. Furthermore, even when operated at 100 mA cm^{-2} it showed the lowest operational time of the bunch, consistently operating for 2-3 h and then suddenly triggering a high voltage spike. The operational voltage started at around 3.6 V, which is also higher than all the other polymers (Fig. 6b). This is coherent with 9C-A-PIP-DAPP having the highest distance in between cations, and lowest cation group concentration. Notably, the selectivity towards CO remained high until failure, although the FE towards gaseous products was the lowest of all the membranes, closing at around 80% (Fig. 6c). A comparable behaviour was observed for 7C-A-PIP-DAPP. This membrane was likewise unable to sustain operation at 200 mA cm^{-2}, and operated for approximately 3-4 h on average at 100 mA cm^{-2} before triggering a voltage spike above 5 V. The selectivity towards CO remained high until failure. The main difference with its longer chain analogue was its operational voltage, which is lower and starts at around 3.35 V at 100 mA cm^{-2}. The lower distance between the cation groups and their higher density is the main reason for this difference. The voltage spike in both these polymers was a peculiar phenomenon which appeared to be reversible. In fact, following a resting period or by recovering the membrane and subsequent retesting, the voltage returned to its initial values (Fig. S11). This suggests that the phenomenon is not due to irreversible chemical degradation, but rather to a reversible behaviour.

The 5C-A-PIP-DAPP membrane operated irregularly at 100 mA cm^{-2}, but the operational lifetime extended up to 20 h, contrary to its longer sidechain equivalents (Fig. S6). Furthermore, this polymer was able to operate at 200 mA cm^{-2}, although its operating voltage fluctuated strongly at this current density as well, exhibiting periodic peaks. The peaks do not cause voltage spikes above 5 V and thus do not necessitate termination of the experiment, enabling direct observation of the reversible and periodic nature of this behaviour. A similar type of voltage spiking has been observed by Hendershot et al. [54], which associated it to drying and rewetting of the interface between the membrane and the cathode. While in their study this dehydration was associated to the low hydration number and water uptake of the membranes, in our case the branched polymers exhibit significantly high hydration numbers, comparatively higher than the linear sidechain ones. The WU of the A-polymers is also higher than 6C-PIP-DAPP. Therefore, this dehydration is more likely related to structural reasons. Although 9C-A-PIP-DAPP had the highest distance between ionic clusters, which could definitely play a part in the sudden dehydration, the comparable ionic cluster distance between 7C-A-PIP-DAPP and 6C-TMA-DAPP seems to suggest there is more to it, as the two polymers have a very similar physical characterisation but the one with the linear sidechain does not show signs of this oscillating voltage behaviour.

EIS during operation at various voltage was performed on all the MEA setups to complement this information (Fig. S12). Firstly, the hierarchy of the various membranes conductivity values is confirmed and reflected in the high-frequency resistance (HFR) values of the respective setups: the setups with 6C-PIP-DAPP, 6C-TMA-DAPP and 5C-A-PIP-DAPP present a lower resistivity than the ones with 7C-A-PIP-DAPP and 9C-A-PIP-DAPP. Importantly, EIS highlighted a clear pattern in the charge-transfer resistance (CTR). The A-polymers, in fact, present a significant CTR at each voltage compared to the negligible CTR of the polymers with linear sidechains and Sustainion. While this could be influenced by multiple aspects such as water uptake, IEC and swelling ratio, the close similarity between all of these properties for some of the branched and some of the linear polymers (e.g. 7C-A-PIP-DAPP and 6C-PIP-DAPP) leads us to conclude that this difference originates mainly from structural reasons associated to the chemical difference between the two polymers: the presence of branching. However, if this was all there is to it, the higher charge-transfer resistance should simply translate to a fixed limiting current due to the sluggish electron transfer, acting as a bottleneck for the reaction mechanism, lower for the polymers with higher CTR. Furthermore, 5C-A-PIP-DAPP should not be able to periodically recover its performance without interrupting the operation. To verify the presence of this limiting current, we performed LSV after the spike on each branched polymer, which did in fact not show an exponential trend. Instead, the current reached a peak and then decreased, which is typical in presence of a limiting current density. This limiting current is systematically higher for the polymers with a higher intrinsic conductivity, and its occurrence reflects transport limitations within the membrane arising from the insufficient number of open ion-conduction pathways. To further analyse the behaviour, LSV was performed on 5C-A-PIP-DAPP at different moments: before operation, right after the spike, and lastly during the moments of operation without spikes (Fig. S10). The results highlighted that the current *vs* potential profiles for 5C-A-PIP-DAPP deviate from the expected exponential trend when the LSV is performed right after the operational voltage spike. However, when the LSV is taken outside of the peaks, the shape of the LSV looks exponential once again, highlighting a change in the limiting current density over time. Thus, we observed that, while this limiting current exists, and it is proportionally lower for 7C-A-PIP-DAPP and 9C-A-PIP-DAPP, it appears to be oscillating over time. To confirm this hypothesis, we tried taking EIS measurements of the 5C-A-PIP-DAPP polymer at operational voltages right after the spiking: when measured after spiking, the EIS shape appears rather chaotic (Fig. S13), but it implies an increase in the charge-transfer resistance and thus a momentary change in the transport behaviour of the membrane. After some recovery time, the EIS measurements go back to the shape and values they had before spiking, once again confirming the transitory nature of this behaviour. To further complement these findings, CA at 3.2 V and 3.7 V was carried out on the A-polymers immediately following voltage spikes. For all the polymers featuring A-type side chains, the notable difference in voltage did not translate to a significant increase in current density (Fig. S14a–b). This test reinforced the hierarchy in conductivity among the three polymer families, with longer sidechains exhibiting lower current densities overall.

A possible suggested explanation is a gradual long-range movement of the polymer's three-dimensional structure during operation due to the lower rotational freedom of the branched sidechains, hindering the sidechain movement. Such reorganisation would reduce the number of available pathways for ion conduction by occlusion of the pathways, thus also hindering water transport, as ion transport and hydrated regions are strictly connected in CO_2 electrolysis. This would also explain the oscillating nature of the limiting current and the transitory variation in the charge-transfer resistance but cannot be directly proven without complex in-situ characterisation of the membrane and thus remains a suggested hypothesis to validate. The reproducibility of the operating time preceding the voltage increase for each distinct setup further supports this hypothesis.

The capability of 5C-A-PIP-DAPP to not exceed 5V even during the spikes and systematically recover the performance shows that the higher conductivity, water uptake and cation group concentration of this type of polymer partially mitigate the performance limitations observed for 7C and 9C, possibly because the really high value of water uptake is

associated to a naturally elevated number of pathways, which could offset and mitigate the theorised less efficient pathway formation and its reorganisation. In fact, under standard operating conditions the setup employing 5C-A-PIP-DAPP has resistivity values comparable to the linear sidechain polymers and its CTR is also the lowest amongst the A-polymers. There are also clear changes in the gaseous product selectivity in correspondence with the voltage peaks, which are realistically connected to the reduced wetting of the cathode side, which allows to reopen the pores of the GDE and to increase the availability of CO_2 on the catalyst surface, partially resetting the selectivity towards CO.

4. Conclusions

This study demonstrates that quaternised DAPP-based AEMs functionalised with a linear sidechain represent promising candidates for CO_2 electrolysis. Among the materials investigated, 6C-PIP-DAPP showed operational properties which were on par - and in some cases superior - to commercial benchmark AEMs, while also exhibiting good stability in alkaline environment, promising long-term operation. Similar remarks can be made for 6C-TMA-DAPP, although its comparatively lower alkaline stability may have limited its durability. In addition, its reduced conductivity leads to slightly higher operational overpotentials when compared to its PIP-based analogue.

In contrast, all membranes with the extra branched methyl group sidechains exhibited underwhelming performance consistency, while also showing some degradation in alkaline environment, rendering them unsuitable for this application. Nevertheless, their study helped unveil a peculiar voltage oscillation behaviour that was studied and characterised. Our main hypothesis suggests it could be connected to the structural role of tertiary carbon adjacent to polymer backbone, possibly impacting the rotational freedom of the sidechains and causing 3D readjustment during operation. This would in turn cause a periodic drying of the cathode interface due to lack of ionic pathways and manifesting as an oscillating limiting current density. Future efforts could aim to better elucidate the dynamics of this behaviour and explore strategies to mitigate its impact.

CRediT authorship contribution statement

Carmelo Parata: Writing – original draft, Methodology, Investigation, Formal analysis, Data curation, Conceptualization. **Antonios Akouros:** Writing – review & editing, Investigation. **Nikolas Theodoropoulos:** Writing – review & editing, Supervision. **Adriano Sacco:** Writing – review & editing, Supervision. **Juqin Zeng:** Writing – review & editing. **Silvia Dante:** Writing – review & editing, Investigation. **Panagiotis Bexis:** Writing – review & editing, Conceptualization. **George Paloumpis:** Writing – review & editing. **Emory S. De Castro:** Writing – review & editing. **Vasiliki Zogali:** Writing – review & editing, Supervision, Investigation, Conceptualization.

Declaration of competing interests

The authors declare the following financial interests/personal relationships which may be considered as potential competing interests: Carmelo Parata reports financial support was provided by European Union. If there are other authors, they declare that they have no known competing financial interests or personal relationships that could have appeared to influence the work reported in this paper.

7. Acknowledgements

This project has received funding from the EU's Horizon 2021 program under the Marie Skłodowska-Curie Doctoral Networks (MSCA-DN) grant agreement No. 101072830. Dr. Christos Chochos is kindly thanked for fruitful discussions during the beginning of the project.

Appendix A. Supplementary data

Supplementary data to this article can be found online at https://doi.org/10.1016/j.memsci.2026.126301.

Data availability

Data will be made available on request.

References

[1] A. Gawel, et al., Electrochemical CO2 reduction-the macroscopic world of electrode design, reactor concepts & economic aspects, iScience 25 (4) (2022) 104011, https://doi.org/10.1016/j.isci.
[2] Z. Zhang, et al., Membrane Electrode Assembly for Electrocatalytic CO2 Reduction: Principle and Application, John Wiley and Sons Inc, Jul. 10, 2023, https://doi.org/10.1002/anie.202302789.
[3] C.M. Gabardo, et al., Continuous carbon dioxide electroreduction to concentrated multi-carbon products using a membrane electrode assembly, Joule 3 (11) (Nov. 2019) 2777–2791, https://doi.org/10.1016/j.joule.2019.07.021.
[4] J. Lin, S. Yan, C. Zhang, Q. Hu, Z. Cheng, "Electroreduction of CO2 Toward High Current Density", MDPI, May 01, 2022 https://doi.org/10.3390/pr10050826.
[5] J. Li, et al., Electrochemical conversion of CO2 to CO utilizing quaternized polybenzimidazole anion exchange membrane, Membranes 13 (2) (Feb. 2023), https://doi.org/10.3390/membranes13020166.
[6] D.A. Salvatore, et al., Designing Anion Exchange Membranes for CO2 Electrolysers, Nature Research, Apr. 01, 2021, https://doi.org/10.1038/s41560-020-00761-x.
[7] X. She, et al., Pure-water-fed, electrocatalytic CO2 reduction to ethylene beyond 1,000 h stability at 10 A, Nat. Energy 9 (1) (Jan. 2024) 81–91, https://doi.org/10.1038/s41560-023-01415-4.
[8] M.A. Blommaert, S. Subramanian, K. Yang, W.A. Smith, D.A. Vermaas, High indirect energy consumption in AEM-Based CO2Electrolyzers demonstrates the potential of bipolar membranes, ACS Appl. Mater. Interfaces 14 (1) (Jan. 2022) 557–563, https://doi.org/10.1021/acsami.1c16513.
[9] X. Hu, et al., An operationally broadened alkaline water electrolyser enabled by highly stable poly(oxindole biphenylene) ion-solvating membranes, Nat. Energy 9 (4) (Apr. 2024) 401–410, https://doi.org/10.1038/s41560-023-01447-w.
[10] H.S. Dang, P. Jannasch, A comparative study of anion-exchange membranes tethered with different hetero-cycloaliphatic quaternary ammonium hydroxides, J. Mater. Chem. A Mater 5 (41) (2017) 21965–21978, https://doi.org/10.1039/c7ta06029g.
[11] H.S. Dang, P. Jannasch, Alkali-stable and highly anion conducting poly(phenylene oxide)s carrying quaternary piperidinium cations, J. Mater. Chem. A Mater 4 (30) (2016) 11924–11938, https://doi.org/10.1039/c6ta01905f.
[12] S. Zhang, et al., Twisted Poly(p-terphenyl-co-m-terphenyl)-Based anion exchange membrane for water electrolysis, ACS Appl. Mater. Interfaces 16 (6) (Feb. 2024) 7660–7669, https://doi.org/10.1021/acsami.3c15525.
[13] T.H. Pham, J.S. Olsson, P. Jannasch, Effects of the: n -alicyclic cation and backbone structures on the performance of poly(terphenyl)-based hydroxide exchange membranes, J. Mater. Chem. A Mater 7 (26) (2019) 15895–15906, https://doi.org/10.1039/c9ta05531b.
[14] F. Wang, Y. Li, C. Li, H. Zhu, Preparation and study of spirocyclic cationic side chain functionalized polybiphenyl piperidine anion exchange membrane, J. Memb. Sci. 620 (2021) 118919, https://doi.org/10.1016/j.memsci.2020.118919.
[15] D. Pan, T.H. Pham, P. Jannasch, Poly(arylene piperidine) anion exchange membranes with tunable N-Alicyclic Quaternary ammonium side chains, ACS Appl. Energy Mater. 4 (10) (Oct. 2021) 11652–11665, https://doi.org/10.1021/acsaem.1c02389.
[16] J. Xue, et al., Chain entanglement and free-volume effects in branched poly(arylene piperidinium) anion-exchange membranes: random-branched versus end-branched, J. Memb. Sci. 717 (2025) 123519, https://doi.org/10.1016/j.memsci.2024.123519.
[17] B. Sana, A. Das, T. Jana, Cross-Linked polybenzimidazoles as alkaline stable anion exchange membranes, ACS Appl. Energy Mater. 5 (3) (Mar. 2022) 3626–3637, https://doi.org/10.1021/acsaem.1c04111.
[18] M. Guo, T. Ban, Y. Wang, X. Wang, Z. Wang, X. Zhu, Polybenzimidazoles incorporating imidazole N-spirocyclic quaternary ammonium cation for anion exchange membranes water electrolysis, J. Memb. Sci. 684 (Oct) (2023), https://doi.org/10.1016/j.memsci.2023.121903.
[19] N. Chen, C. Hu, H.H. Wang, J.H. Park, H.M. Kim, Y.M. Lee, Chemically & physically stable crosslinked poly(aryl-co-aryl Piperidinium)s for anion exchange membranes fuel cells, J. Memb. Sci. 638 (2021) 119685, https://doi.org/10.1016/j.memsci.2021.119685.
[20] A. Allushi, P.M. Bakvand, H. Gong, P. Jannasch, Hydroxide conducting BAB triblock copolymers tailred for durable high-performance anion exchange membranes, Mater. Adv. 4 (17) (2023) 3733–3745, https://doi.org/10.1039/D3MA00207A.
[21] Y. Zhao, H. Yu, D. Xing, W. Lu, Z. Shao, B. Yi, Preparation and characterization of PTFE based composite anion exchange membranes for alkaline fuel cells, J. Memb. Sci. 421–422 (2012) 311–317, https://doi.org/10.1016/j.memsci.2012.07.034.
[22] M. Moreno-González, et al., One year operation of an anion exchange membrane water electrolyzer utilizing Aemion+® membrane: minimal degradation, low H2

crossover and high efficiency, J. Power Sources Adv. 19 (Jan. 2023) 100109, https://doi.org/10.1016/J.POWERA.2023.100109.
[23] J. Wang, et al., Poly(aryl piperidinium) membranes and ionomers for hydroxide exchange membrane fuel cells, Nat. Energy 4 (5) (May 2019) 392–398, https://doi.org/10.1038/s41560-019-0372-8.
[24] Kim, et al., Efficient and stable CO2 reduction using quaternary ammonium-based high-durability polymer membrane and ionomer in zero-gap electrolyzers, J. Membr. Sci. 738 (Part A) (2026) 124724, https://doi.org/10.1016/j.memsci.2025.124724.
[25] M.M. Shanbhag, S. Mishra, N.P. Shetti, T. Palanivel, S.S. Kalanur, B.G. Pollet, Advancements and Challenges in Anion Exchange Membrane Technology for Sustainable Energy Applications, Elsevier Ltd., Oct. 01, 2025, https://doi.org/10.1016/j.mtener.2025.101976.
[26] W.H. Lee, E.J. Park, J. Han, D.W. Shin, Y.S. Kim, C. Bae, Poly(terphenylene) anion exchange membranes: the effect of backbone structure on morphology and membrane property, ACS Macro Lett. 6 (5) (May 2017) 566–570, https://doi.org/10.1021/acsmacrolett.7b00148.
[27] E.J. Park, Y.S. Kim, Quaternized Aryl Ether-free Polyaromatics for Alkaline Membrane Fuel Cells: Synthesis, Properties, and performance-a Topical Review, Royal Society of Chemistry, 2018, https://doi.org/10.1039/c8ta05428b.
[28] J.Y. Jeon, et al., Synthesis of aromatic anion exchange membranes by friedel-crafts bromoalkylation and cross-linking of polystyrene block copolymers, Macromolecules 52 (5) (Mar. 2019) 2139–2147, https://doi.org/10.1021/acs.macromol.8b02355.
[29] D. Henkensmeier, M. Najibah, C. Harms, J. Žitka, J. Hnát, K. Bouzek, Overview: state-of-the art commercial membranes for anion exchange membrane water electrolysis, J. Electrochem. Energy Convers. Storage 18 (2) (May 2021), https://doi.org/10.1115/1.4047963.
[30] W. Song, et al., Alkaline membranes toward electrochemical energy devices: recent development and future perspectives, ACS Cent. Sci. 9 (8) (Aug. 2023) 1538–1557, https://doi.org/10.1021/acscentsci.3c00597.
[31] C. Fujimoto, D.S. Kim, M. Hibbs, D. Wrobleski, Y.S. Kim, Backbone stability of quaternized polyaromatics for alkaline membrane fuel cells, J. Memb. Sci. 423–424 (Dec. 2012) 438–449, https://doi.org/10.1016/j.memsci.2012.08.045.
[32] E.J. Park, S. Maurya, M.R. Hibbs, C.H. Fujimoto, K.D. Kreuer, Y.S. Kim, Alkaline stability of quaternized diels-alder polyphenylenes, Macromolecules 52 (14) (Jul. 2019) 5419–5428, https://doi.org/10.1021/acs.macromol.9b00853.
[33] M.R. Hibbs, Alkaline stability of poly(phenylene)-based anion exchange membranes with various cations, J. Polym. Sci. B Polym. Phys. 51 (24) (Dec. 2013) 1736–1742, https://doi.org/10.1002/polb.23149.
[34] C. Hu, Y. Wang, Y.M. Lee, Ether-Free Alkaline Polyelectrolytes for Water Electrolyzers: Recent Advances and Perspectives, John Wiley and Sons Inc, Jan. 15, 2025, https://doi.org/10.1002/anie.202418324.
[35] C.H. Fujimoto, M.A. Hickner, C.J. Cornelius, D.A. Loy, Ionomeric poly(phenylene) prepared by Diels-Alder polymerization: synthesis and physical properties of a novel polyelectrolyte, Macromolecules 38 (12) (Jun. 2005) 5010–5016, https://doi.org/10.1021/ma0482720.
[36] Y. Zhang, et al., Tuning hydrogen bond and flexibility of N-spirocyclic cationic spacer for high performance anion exchange membranes, J. Memb. Sci. 613 (2020), https://doi.org/10.1016/j.memsci.2020.118507.
[37] K.M. Hugar, W. You, G.W. Coates, Protocol for the quantitative assessment of organic cation stability for polymer electrolytes, ACS Energy Lett. 4 (7) (Jul. 2019) 1681–1686, https://doi.org/10.1021/acsenergylett.9b00908.
[38] Z. Tao, C. Wang, X. Zhao, J. Li, M.D. Guiver, "Progress in High-Performance Anion Exchange Membranes Based on the Design of Stable Cations for Alkaline Fuel Cells", John Wiley and Sons Inc, May 01, 2021 https://doi.org/10.1002/admt.202001220.
[39] J.Y. Jeon, D. Tian, M.K. Pagels, C. Bae, Efficient preparation of styrene block copolymer anion exchange membranes via one-step friedel-crafts bromoalkylation with alkenes, Org. Process Res. Dev. 23 (8) (Aug. 2019) 1580–1586, https://doi.org/10.1021/acs.oprd.9b00218.
[40] T.H. Pham, A. Allushi, J.S. Olsson, P. Jannasch, Rational molecular design of anion exchange membranes functionalized with alicyclic quaternary ammonium cations, Polym. Chem. 11 (43) (Nov. 2020) 6953–6963, https://doi.org/10.1039/d0py01291b.
[41] S.S. Sekhon, J.S. Park, Y.W. Choi, A SAXS study on nanostructure evolution in water free membranes containing ionic liquid: from dry membrane to saturation, Phys. Chem. Chem. Phys. 12 (41) (Nov. 2010) 13763–13769, https://doi.org/10.1039/c0cp00966k.
[42] T.H. Pham, J. Olsson, P. Jannasch, N-Spirocyclic Quaternary ammonium ionenes for anion-exchange membranes, J. Am. Chem. Soc. 139 (8) (2017) 2888–2891, https://doi.org/10.1021/jacs.6b12944.
[43] J.S. Olsson, T.H. Pham, P. Jannasch, Functionalizing polystyrene with N-Alicyclic piperidine-based cations via friedel-crafts alkylation for highly alkali-stable anion-exchange membranes, Macromolecules 53 (12) (Jun. 2020) 4722–4732, https://doi.org/10.1021/acs.macromol.0c00201.
[44] L. Ge, et al., Electrochemical CO2 Reduction in membrane-electrode Assemblies, Elsevier Inc, Mar. 10, 2022, https://doi.org/10.1016/j.chempr.2021.12.002.
[45] M. Liu, X. Hu, B. Hu, L. Liu, N. Li, Soluble poly(aryl piperidinium) with extended aromatic segments as anion exchange membranes for alkaline fuel cells and water electrolysis, J. Memb. Sci. 642 (2022) 119966, https://doi.org/10.1016/j.memsci.2021.119966.
[46] M. Guo, T. Ban, Y. Wang, X. Wang, X. Zhu, 'Thiol-ene' crosslinked polybenzimidazoles anion exchange membrane with enhanced performance and durability, J. Colloid Interface Sci. 638 (May 2023) 349–362, https://doi.org/10.1016/j.jcis.2023.01.137.
[47] H. Zhang, X. He, H. Feng, C. Li, M. Li, A poly(binaphthyl-co-terphenyl quinuclidinium) anion exchange membrane with excellent alkaline stability and anion conductivity, J. Mater. Chem. A Mater 12 (35) (Aug. 2024) 23570–23576, https://doi.org/10.1039/d4ta03241a.
[48] K.M. Meek, J.R. Nykaza, Y.A. Elabd, Alkaline chemical stability and ion transport in polymerized ionic liquids with various backbones and cations, Macromolecules 49 (9) (May 2016) 3382–3394, https://doi.org/10.1021/acs.macromol.6b00434.
[49] M.G. Marino, K.D. Kreuer, Alkaline stability of quaternary ammonium cations for alkaline fuel cell membranes and ionic liquids, ChemSusChem 8 (3) (2015) 513–523, https://doi.org/10.1002/cssc.201403022.
[50] O. Bostrom, S.-Y. Choi, L. Xia, S. Meital, F. Lohmann-Richters, P. Jannash, Alkali-stable polybenzimidazole anion exchange membranes tethered with N,N-dimethylpiperidinium cations for dilute aqueous KOH fed water electrolyzers, J. Mater. Chem. A 11 (39) (2023) 21170–21182, https://doi.org/10.1039/D3TA03216G.
[51] R.B. Kutz, Q. Chen, H. Yang, S.D. Sajjad, Z. Liu, I.R. Masel, Sustainion imidazolium-functionalized polymers for carbon dioxide electrolysis, Energy Technol. 5 (6) (Jun. 2017) 929–936, https://doi.org/10.1002/ente.201600636.
[52] Z. Liu, H. Yang, R. Kutz, R.I. Masel, CO2 electrolysis to CO and O2 at high selectivity, stability and efficiency using sustainion membranes, J. Electrochem. Soc. 165 (15) (2018) J3371–J3377, https://doi.org/10.1149/2.0501815jes.
[53] G.O. Larrazábal, et al., Analysis of mass flows and membrane cross-over in CO2 reduction at high current densities in an MEA-type electrolyzer, ACS Appl. Mater. Interfaces 11 (44) (Nov. 2019) 41281–41288, https://doi.org/10.1021/acsami.9b13081.
[54] J. Hendershot, et al., Anion exchange membrane transport and accelerated lifetime testing of membrane electrode assembly cells for the electrochemical reduction of CO 2 -to-C 2 products, J. Electrochem. Soc. 172 (9) (Sep. 2025) 094509, https://doi.org/10.1149/1945-7111/ae041b.
[55] L. Weseler, T. Brands, R. Gustus, T. Turek, Benchmarking anion exchange membranes and ionomers for electrochemical CO_2 reduction, ACS Appl. Energy Mater. 9 (7) (2026) 4359–4372, https://doi.org/10.1021/acsaem.6c00327.